

PAPER

Energy harvesting properties of the Nafion thin films

To cite this article: Anjaly Babu *et al* 2022 *Eng. Res. Express* **4** 045015

View the [article online](#) for updates and enhancements.

You may also like

- [Influence of Equivalent Weight of Ionomer on Proton Conduction Behavior in Fuel Cell Catalyst Layers](#)
Shuiyun Shen, Aidi Han, Xiaohui Yan et al.
- [Combining electrodermal activity analysis and dynamic causal modeling to investigate the visual-odor multimodal integration during face perception](#)
Gianluca Rho, Alejandro Luis Callara, Francesco Bossi et al.
- [Fitting of Low-Pt PEM Fuel Cell Polarization Curves by Means of a Single-Pore Catalyst Layer Model](#)
Andrei Kulikovskiy

Engineering Research Express



PAPER

Energy harvesting properties of the Nafion thin films

RECEIVED
1 June 2022

REVISED
23 September 2022

ACCEPTED FOR PUBLICATION
28 October 2022

PUBLISHED
7 November 2022

Anjaly Babu¹ , P Supraja¹ , Siju Mishra¹ , K Uday Kumar^{1,*} , R Rakesh Kumar^{1,*} , D Haranath¹ ,
C Thirimal² , N Raju³ , T Venkatappa Rao¹ , K Balaji⁴ and A Rajanikanth⁴

¹ Department of Physics, Energy Materials and Devices Lab, National Institute of Technology Warangal, 506004, India

² Centre for Nanoscience and Technology, Department of Physics, VNR VJIEET, Hyderabad, 500090, India

³ Department of Physics, Osmania University, Hyderabad, 500007, India

⁴ School of Physics, University of Hyderabad, Hyderabad, Telangana 500046, India

* Authors to whom any correspondence should be addressed.

E-mail: kanapuram.udaykumar@nitw.ac.in and rakeshr@nitw.ac.in

Keywords: polymers, electron microscopy, piezoionic effect, nanogenerators, biomechanical energy, energy harvesting

Supplementary material for this article is available [online](#)

Abstract

In this report, energy harvesting properties of Nafion films were investigated using piezoionic generator (PIOG) and triboelectric generator (TEG) devices. Nafion films were prepared by simple doctor blade deposition of a Nafion ionomer solution onto the aluminum electrode. The Nafion films were characterized for their surface morphology, composition, and crystallinity. Furthermore, the Nafion film exhibited strong substrate adhesion, a smooth surface, and amorphous nature. The deposited Nafion film was used directly as an active layer to fabricate the PIOG and TEG devices with ITO electrodes. Output voltages of ~ 450 mV and ~ 1.9 V have been observed for the PIOG and TEG devices against biomechanical energy. The maximum instantaneous power produced by these devices is approximately $\sim 0.205 \mu\text{W cm}^{-2}$, and $\sim 0.128 \mu\text{W cm}^{-2}$ for the PIOG and TEG, respectively. The PIOG performance can be further improved using Nafion composite films. Similarly, the TEG performance can be enhanced with other friction layers such as PVDF, PDMS, PMMA, and PVC films instead of ITO. Therefore, the proposed nanogenerators can be used as touch sensors and energy sources for wearable electronic devices in the future.

1. Introduction

Energy harvesting from the environment (e.g., solar, thermal, wind, tidal, and mechanical energy) is cost-effective for sustainable economic growth and environmental concerns [1, 2]. Scavenging ubiquitous yet unexplored forms of mechanical energy from the surroundings has recently gained research interest owing to its easy availability in daily life. Triboelectric and piezoelectric energy harvesting devices have been developed to scavenge mechanical energy [3, 4]. These devices convert ambient mechanical energy into electrical energy and power portable electronic devices, sensors, healthcare, and Internet of Things (IoT) systems [5, 6]. In piezoelectric energy harvesting, electrical output is generated due to the re-orientation of molecular dipole moments with mechanical force [7]. In triboelectric energy harvesting, two dissimilar materials with opposite electron affinities produce electrical energy due to the coupling effect of contact electrification and electrostatic induction [8–10]. The major drawback of these devices is their low output powers. Currently, research focuses on developing high-performance energy harvesting devices using different strategies [11, 12]. Common strategies for both devices include testing/using new materials or material composites [13, 14] and poling the materials [15, 16]. In the case of TENG, other strategies, such as increasing the effective contact area, surface charge density, and device size, have been used to enhance the performance of TEG devices [17–19]. In the present study, exploring new materials has been adopted for energy harvesting devices. A new material Nafion was selected to fabricate energy harvesting devices using piezoionic effect and triboelectric effects. Nafion is the generic name for a sulfonated tetrafluoroethylene-based fluoropolymer-copolymer. Nafion has been used extensively in fuel cells as an excellent proton exchange membrane [20], in fuel cell applications [21, 22],

actuators [23–27] supercapacitors [28], sensors [29], and energy harvesting [30–35]. In actuator applications, not only pure Nafion but also Nafion composites such as Nafion-ZnO [36], and Nafion-CNT composite films were used to enhance the actuation response [37]. It is also used in a wide range of applications like electrode modifiers for sensor fabrication [38, 39], biosensors [40], controlled drug release [41], formation of an antimicrobial coating [42], fluorine magnetic resonance imaging [43], gas drying [44], and catalysis [45, 46]. Recently, Self-charging supercapacitor power cells (SCSPCs) were demonstrated using piezoionic properties of Nafion films [47]. These devices can be charged via mechanical stimulation due to the piezoelectric effect of the separator. These SCSPCs have high potential applications in self-powered wearable healthcare monitoring devices.

Only limited reports are available on the energy harvesting properties of Nafion polymer to the best of our knowledge [30–35]. In a few reports, energy harvesting has been done from an ocean wave, underwater vibration. In other reports, Nafion-filled PVDF films were used for energy harvesting. In all the reports, the piezoelectric property of the Nafion polymer is utilized. However, Nafion film-based triboelectric energy harvesting was not reported so far, and the present manuscript reports the same. In addition, most reports directly utilized the Nafion membrane for energy harvesting. Whereas in this manuscript, Nafion films are prepared using the doctor blade method, and this was not reported earlier in the literature. There are reports on energy harvesting devices using polymers such as polyvinylidene fluoride (PVDF), its copolymers (PVDF-TrFE), polydimethylsiloxane (PDMS), nylon, and PVA [48, 49]. These devices utilized the piezoelectric and triboelectric effects. The dielectric and induced charges are responsible for energy conversion in the case of piezoelectric and triboelectric effects. In contrast, in the piezoionic effect, an electrical voltage is generated in response to mechanical deformation with the mechanism of ion redistribution in specific ionic polymers and polymer composites [29, 50, 51].

The present manuscript reports the energy harvesting properties of Nafion polymer film prepared by the doctor blade coating technique. The fabricated piezoionic generator (PIOG) and triboelectric generator (TEG) devices are demonstrated for bio-mechanical energy harvesting applications.

2. Experimental: materials and methods

2.1. Materials

A perfluorinated resin solution containing Nafion 1100W-20 wt. % ionomer procured commercially from Dupont, Tin doped indium oxide (ITO) PET substrates with sheet resistance ($10 \Omega/\square$) obtained from Sigma Aldrich and used as conducting electrodes. The aluminum (Al) foil of 0.1 mm of thickness was procured from $M s^{-1}$ Special Metals Pvt. Ltd, India.

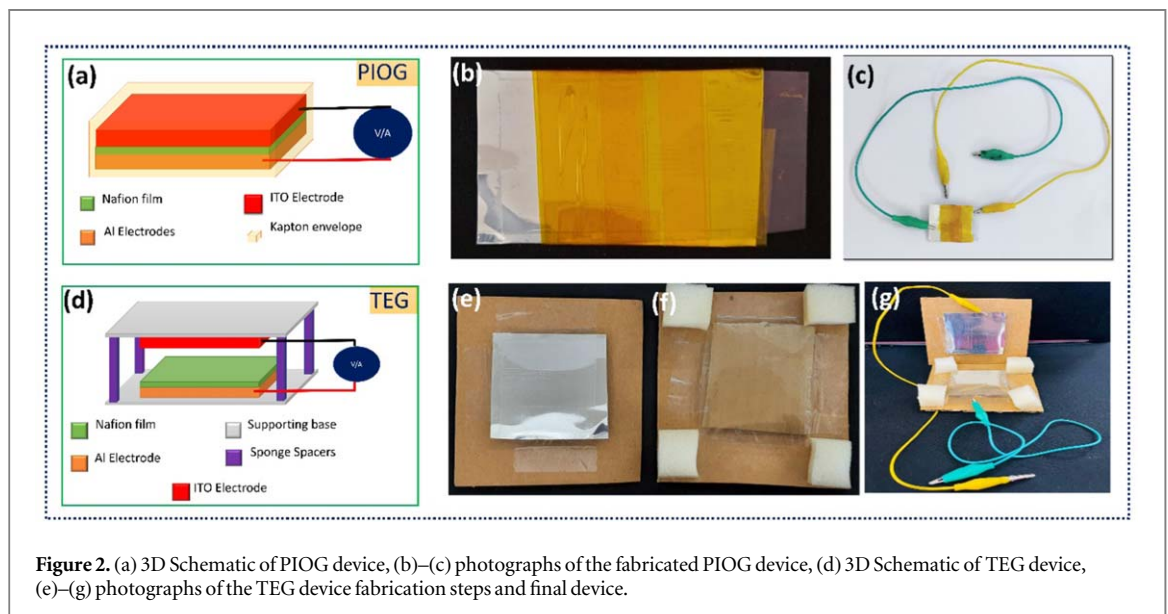
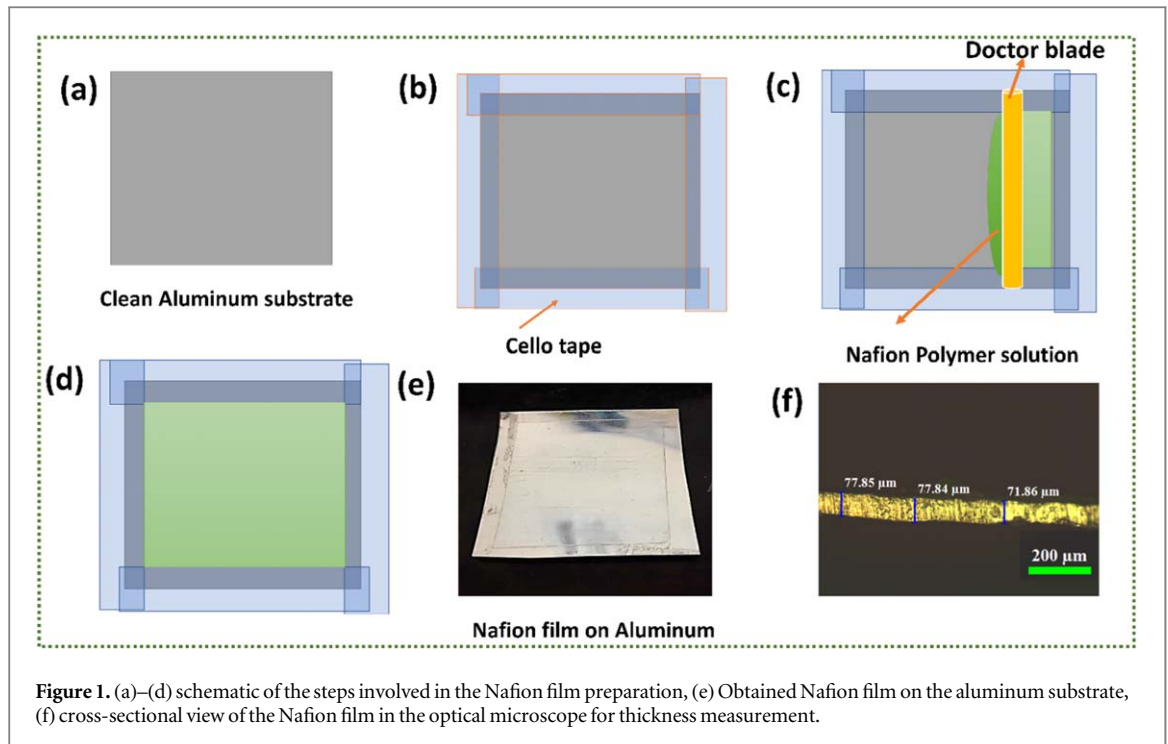
2.2. Preparation and characterization details of nafion films

The Nafion perfluorinated resin solution was directly coated on clean Al substrates using the doctor blade coating technique. Figures 1(a)–(d) show the deposition process steps schematics. Before Nafion film deposition, a clean aluminum substrate was masked on four sides, as shown in the schematic in figure 1(b), to obtain a uniform shape and thickness of the film.

The masked substrate was placed on the smooth glass to support the substrate during the doctor-blading operation. Nafion solution was initially dropped onto the Al substrate, and a spreader was driven through the solution at a blade speed of 30 mm s^{-1} . The obtained films were dried for 6 h, and the masked portions were removed for electrode connections. Figure 1(e) shows the photograph of the transparent Nafion film obtained on the substrate. Figure 1(f) shows the cross-sectional view of the Nafion film captured using an optical microscope (Olympus BX53). The Nafion film thickness was measured at different locations from the cross-sectional view of the Nafion film and was found to be $\sim 75 \mu\text{m}$. The prepared Nafion film's crystallinity, morphology, and composition were characterized using X-ray diffraction (XRD, Bruker D8) and scanning electron microscopy (SEM, ZEISS). Fourier transform infrared spectroscopy (FTIR-4200) was used for the identification of functional groups present in the Nafion film. Raman spectroscopy was performed using Horiba Jobin Yvon Micro Raman HR800, using 532 nm He-Ne laser as the excitation source.

2.3. PIOG and TEG device fabrication and testing procedure

The schematics of both devices are shown in figures 2(a) and (d). The PIOG device ($2 \text{ cm} \times 3 \text{ cm}$) was fabricated by keeping the ITO electrode on the Nafion film surface and was sealed perfectly using Kapton tape to avoid slight movement and shorting problems (figure 2(b)). For the TEG device preparation ($5 \text{ cm} \times 5 \text{ cm}$), the PET/ITO electrode film and Nafion deposited substrate was placed on cardboard support, as shown in figures 2(e)–(f). In the next step, a sponge spacer was positioned such that a distance of 3 cm separates the Nafion and the top electrode. Two connecting wires were attached to the aluminum and ITO in both devices, as shown in



figures 2(c) and (d), respectively, to record the output voltage. The open-circuit voltage (V_{oc}) was measured using a digital oscilloscope (TBS1102) with an input impedance of $1\text{ M}\Omega$. Furthermore, the output power and stability of PIQG and TEG devices have been studied.

3. Results and discussions

3.1. Nafion thin film characterization

Figures 3(a)–(b) shows the surface morphology of the Nafion film at low and high magnifications. The Nafion film surface is smooth overall, with a rough surfaces in a few places. Figure 3(c) shows the EDX spectrum of the Nafion film, which reveals the presence of carbon, sulfur, and fluorine without any other impurity elements. Figure 3(d) shows the XRD pattern of Nafion films coated on an Aluminum substrate, and it has two diffraction peaks related to the Nafion at $2\theta = 16.5$ and 39.5° . The first diffraction peak ($2\theta = 16.5^\circ$) is associated with the crystalline peak of Nafion, and the second diffraction peak ($2\theta = 39.5^\circ$) refers to polyfluorocarbon chains in the Nafion structure [52, 53]. The Raman spectra of the Nafion film is as shown in figure 3(e). The peaks around

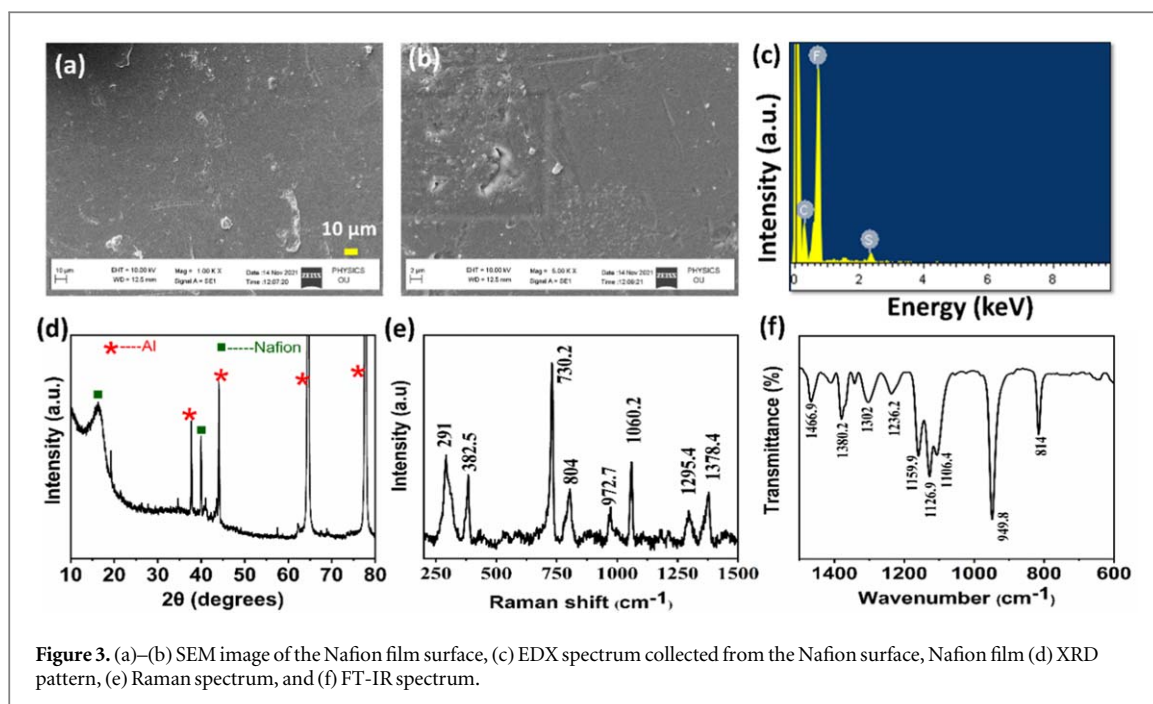


Figure 3. (a)–(b) SEM image of the Nafion film surface, (c) EDX spectrum collected from the Nafion surface, Nafion film (d) XRD pattern, (e) Raman spectrum, and (f) FT-IR spectrum.

1060, 972.7, and 804 cm^{-1} originate from the stretching vibrations of S–O, C–O, and S–C in the Nafion side chains. The peaks observed at 730.5 cm^{-1} correspond to symmetric stretching vibrations of CF_2 . The peaks observed at 382.5 and 291 cm^{-1} correspond to the wagging vibration mode of SO_2 and the twisting vibration of CF_2 , respectively. The C–C single bond peaks were observed around 1295.4 and 1378.4 cm^{-1} . The Raman spectrum of the Nafion membrane is consistent with previous reports [54, 55]. Figure 3(f) shows the FTIR spectrum of the Nafion. The transmittance band at 1236 cm^{-1} and 1126, 1153 cm^{-1} is due to the symmetric and asymmetric vibrations of CF_2 , respectively. The peak around 814 cm^{-1} is due to the symmetric stretching vibrations of the C–S group. The small peak observed at 1053 cm^{-1} , and 982.2 cm^{-1} are attributed to the symmetric SO_3^- stretching vibration and C–O–C linkage [56]. The peak observed at 1410.9 cm^{-1} is assigned an anti-symmetric stretching $S = 0$ band in the $-\text{SO}_3\text{H}$ group. The transmittance peak at 1302 cm^{-1} corresponds to the CF_2 stretching vibration [57]. At 1466.9 cm^{-1} , the asymmetric peak is due to the combination of C-F bands that occurs at the 1420 cm^{-1} and 1450 cm^{-1} of the amorphous PTFE [58].

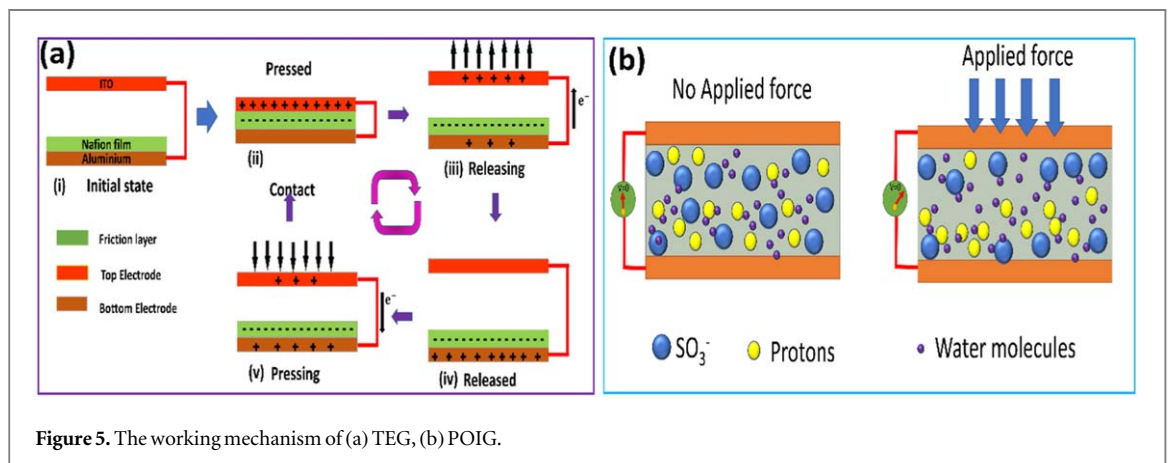
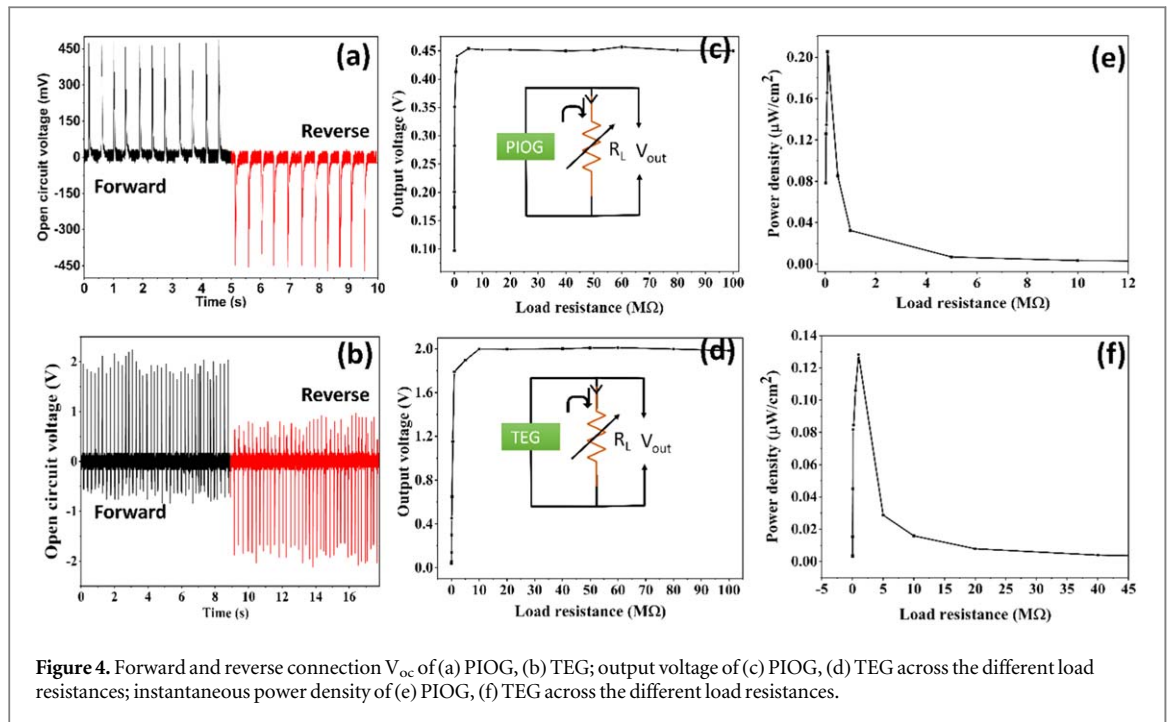
3.2. PIOG and TEG device performance

The V_{oc} values of PIOG (finger tapping) and TEG (hand tapping) for repeated application of biomechanical force are presented in figures 4(a) and (b), respectively. For each tapping, the V_{oc} of ~ 450 mV and ~ 1.9 V were observed for PIOG and TEG devices. In the PIOG, finger tapping induces deformation of the Nafion film. Consequently, ions are redistributed and produce a potential difference [29]. In a TEG, voltage is generated owing to contact electrification and electrostatic induction [6].

Further, a switching polarity test was performed for both devices by reversing the connections to the oscilloscope [59]. The response signals of the PIOG and TEG in both connection geometries are opposite with respect to the previous signal, and this confirms the output generated by the PIOG and TEG devices alone, not from the instrument noise. Noise cannot change polarity upon reversal of the connection. In addition to the switching polarity test, a linear superposition of the voltage test was performed using two series-connected PIOG devices. The resultant voltage of the series-connected PIOG devices (~ 900 mV) is almost double the single device voltage (~ 450 mV) (See supplementary information, S1) [59, 60].

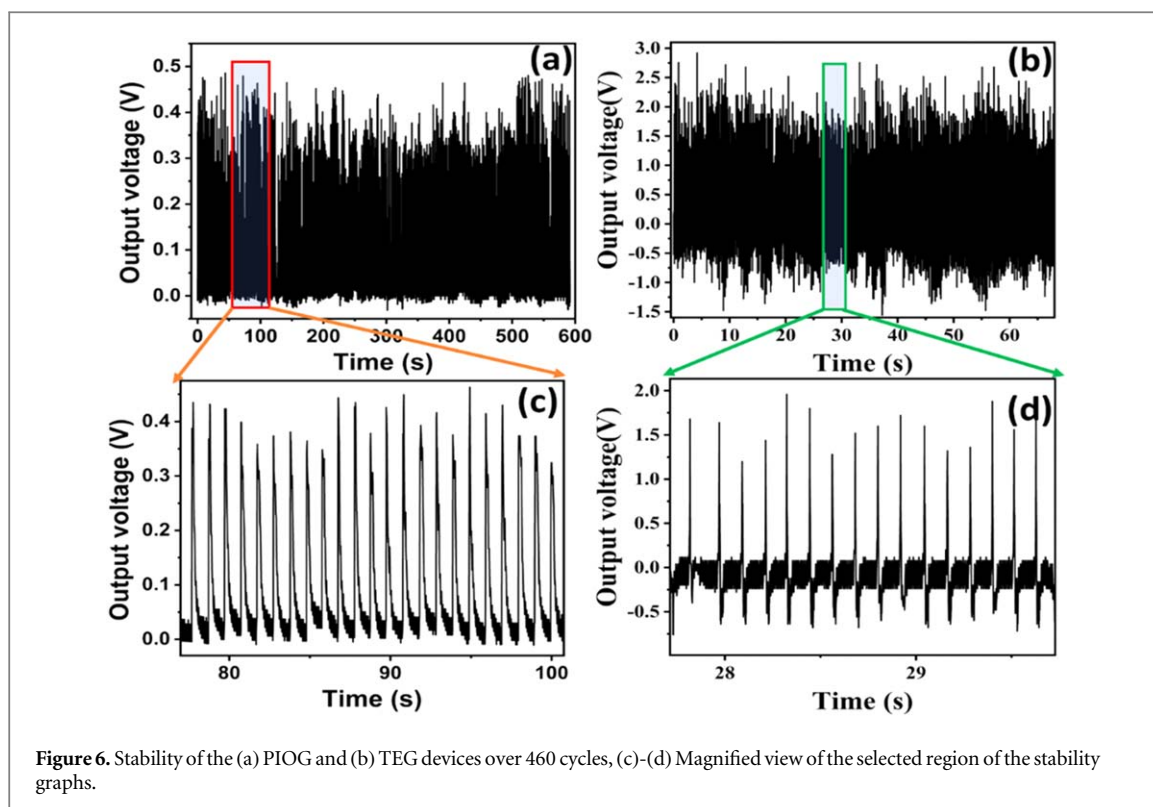
Further, the nanogenerator's output voltage was measured across different load resistance values (10 k Ω to 100 M Ω) to calculate the instantaneous power and power density of the PIOG and TEG devices (See supplementary information, S2). The output voltages of PIOG (finger tapping), TEG (hand tapping) at different load resistance values are presented in figures 4(c) and (d), respectively.

The output voltage increased with the load resistance and saturated at a higher value of resistances for both devices. The saturation voltage of ~ 454 mV and ~ 1.9 V were observed at load resistance values of 5 M Ω and 10 M Ω for PIOG and TEG, respectively. The difference in the saturation in output voltage at different load resistance values for PIOG and TEG is due to their different internal resistances. The PIOG and TEG devices have different device resistances due to the different sizes of the devices. Further, instantaneous power density ($P = V^2/(A \cdot R_L)$) values nanogenerators are calculated and presented in figures 4(e)–(f). The power density



characteristics of PIOG, and TEG is in good agreement with the previously reported literature [61, 62]. The maximum instantaneous output power density of $\sim 0.205 \mu\text{W cm}^{-2}$, $0.128 \mu\text{W cm}^{-2}$ at load resistance values of $\sim 100 \text{K}\Omega$, $1 \text{M}\Omega$ for PIOG and TEG, respectively.

The operating principle of polymer-based triboelectric generators has been well explained in the literature, and the exact mechanism is adopted in this study [63–66]. A schematic description of electrical energy generation based on contact electrification and electrostatic induction is presented in figure 5(a). The TEG is in equilibrium at the initial state because there is no contact between the top ITO electrode and Nafion film (figures 5(a) (i)). When an external force is applied to the TEG, these layers come into contact, and they exchange charges based on their electron affinities to lose or gain charges. Nafion carries a negative charge, while the ITO electrode carries the same amount of positive charge, keeping the TEG in a balanced state (figures 5(a) (ii)). An electric potential is induced between the TEG's top and bottom electrodes when the external force is removed due to electrostatic induction. This potential difference drives the electrons from the bottom electrode to the top electrode through the load resistance until the equilibrium state is reached. (figures 5(a) (iii)–(iv)). When an external force was applied again, the electrostatically induced charges flowed back from the top electrode to the bottom electrode and reached a balanced state (figures 5(a) (v)). When the ITO and Nafion films are in complete contact again, all induced charges are neutralized, and the TEG returns to the equilibrium state. This process of the pressing and releasing cycle produces an AC electrical output. In the case of the PIOG device, protons and sulfonic ions are randomly distributed in the Nafion polymer in the absence of external force, which results in



zero potential across the electrodes. When force is applied to the POIG device, the potential difference is generated due to the redistribution of protons and sulfonic ions in the Nafion film, as shown in figure 5(b).

Furthermore, the stability of the nanogenerator was tested over 460 cycles, and responses are shown in figures 6(a)–(b). Figures 6(c)–(d) represent the magnified views of the selected regions of the stability graphs. The high stability of PIOG, and TEG can be evidenced in figure 6.

4. Conclusions

In summary, piezoionic and triboelectric generators were fabricated using Nafion films, and their energy harvesting properties were studied. The fabricated PIOG device exhibited an open-circuit voltage and output power density of ~ 450 mV and $\sim 0.205 \mu\text{W cm}^{-2}$ against finger tapping. Similarly, the fabricated TEG device has shown open-circuit voltage and output power density of ~ 1.9 V and $\sim 0.128 \mu\text{W cm}^{-2}$, against hand tapping, respectively. These two devices exhibited excellent stability over many test cycles. Further investigations are required to understand the piezoionic effect more clearly and improve the performance of PIOG and TEG devices.

Acknowledgments

The authors would like to thank the Department of Physics and Centre for Research and Instrument facility (CRIF), NIT-Warangal, for providing their research facilities. The authors would like to thank Dr. V. Jayalaxmi, Dept.Of. Physics, NIT-Warangal for extending microscope facility.

Data availability statement

All data that support the findings of this study are included within the article (and any supplementary files).












Funding statement

The authors declare that there is funding for this research work.

Conflict of interest statement

The authors declare that they have no known competing financial interests.

ORCID iDs

Anjaly Babu  <https://orcid.org/0000-0001-9569-7442>
P Supraja  <https://orcid.org/0000-0001-5612-4035>
Siju Mishra  <https://orcid.org/0000-0003-3774-4196>
K Uday Kumar  <https://orcid.org/0000-0003-1297-4104>
R Rakesh Kumar  <https://orcid.org/0000-0003-4023-9051>
D Haranath  <https://orcid.org/0000-0002-7936-6165>
C Thirmal  <https://orcid.org/0000-0002-4211-3009>
N Raju  <https://orcid.org/0000-0001-8004-2291>
T Venkatappa Rao  <https://orcid.org/0000-0003-4978-7011>
K Balaji  <https://orcid.org/0000-0003-4631-2619>
A Rajanikanth  <https://orcid.org/0000-0002-5871-6656>

References

- [1] Wang H, Jasim A and Chen X 2018 Energy harvesting technologies in roadway and bridge for different applications—a comprehensive review *Appl. Energy* **212** 1083–94
- [2] Ahmadi M H, Ghazvini M, Nazari M A, Ahmadi M A, Pourfayaz F, Lorenzini G and Ming T 2019 Renewable energy harvesting with the application of nanotechnology: a review *Int. J. Energy Res.* **43** 1387–410
- [3] Briscoe J and Dunn S 2014 Piezoelectric nanogenerators—a review of nanostructured piezoelectric energy harvesters *Nano Energy* **14** 15–29
- [4] Wang Z L 2021 From contact electrification to triboelectric nanogenerators *Rep. Prog. Phys.* **84** 96502
- [5] Zhang C, Fan W, Wang S, Wang Q, Zhang Y and Dong K 2021 Recent progress of wearable piezoelectric nanogenerators *ACS Appl Electron Mater* **3** 2449–67
- [6] Zhou L, Liu D, Wang J and Wang Z L 2020 Triboelectric nanogenerators: fundamental physics and potential applications **8** 481–506
- [7] Anton S R and Sodano H A 2007 A review of power harvesting using piezoelectric materials (2003–2006) *Smart Mater. Struct.* **16** R1
- [8] Luo J and Wang Z L 2020 Recent progress of triboelectric nanogenerators: from fundamental theory to practical applications *EcoMat* **2** 1–22
- [9] Wang Z L 2017 On Maxwell's displacement current for energy and sensors: the origin of nanogenerators *Mater. Today* **20** 74–82
- [10] Lin Z, Chen J and Yang J 2016 Recent progress in triboelectric nanogenerators as a renewable and sustainable power source *J. Nanomater.* **2016** 1–24
- [11] Le A T, Ahmadipour M and Pung S-Y 2020 A review on ZnO-based piezoelectric nanogenerators: synthesis, characterization techniques, performance enhancement and applications *J. Alloys Compd.* **844** 156172
- [12] Liu W, Wang Z and Hu C 2021 Advanced designs for output improvement of triboelectric nanogenerator system *Mater. Today* **45** 93–119
- [13] Liu H, Zhong J, Lee C, Lee S W and Lin L 2018 A comprehensive review on piezoelectric energy harvesting technology: materials, mechanisms, and applications *Appl. Phys. Rev.* **5** 041306
- [14] Zhang R and Olin H 2020 Material choices for triboelectric nanogenerators: a critical review *Eco. Mat.* **2** 1–13
- [15] Ali D, Yu B, Duan X, Yu H and Zhu M 2017 Enhancement of output performance through post-poling technique on BaTiO₃/PDMS-based triboelectric nanogenerator *Nanotechnology* **28** 075203
- [16] Ippili S, Jella V, Kim J, Hong S and Yoon S G 2018 Enhanced piezoelectric output performance via control of dielectrics in Fe₂+ incorporated MAPbI₃ perovskite thin films: flexible piezoelectric generators *Nano Energy* **49** 247–56
- [17] Wang S, Xie Y, Niu S, Lin L, Liu C, Zhou Y S and Wang Z L 2014 Maximum surface charge density for triboelectric nanogenerators achieved by ionized-air injection: methodology and theoretical understanding *Adv. Mater.* **26** 6720–8
- [18] Mahmud M A P, Lee J J, Kim G H, Lim H J and Choi K B 2016 Improving the surface charge density of a contact-separation-based triboelectric nanogenerator by modifying the surface morphology *Microelectron. Eng.* **159** 102–7
- [19] Supraja P, Kumar R R, Mishra S, Haranath D, Sankar P R, Prakash K, Jayarambabu N, Rao T V and Kumar K U 2022 A simple and low-cost triboelectric nanogenerator based on two dimensional ZnO nanosheets and its application in portable electronics *Sens Actuators A Phys.* **335** 113368
- [20] Peighambaridoust S J, Rowshanzamir S and Amjadi M 2010 *Review of the proton exchange membranes for fuel cell applications* **35** 9349–84
- [21] Choi E, Kim S M and Jang S 2022 Highly durable membrane electrode assembly with multiwalled carbon nanotubes/CeO₂-reinforced nafion composite membrane by spraying method for fuel cell applications *Adv. Mater. Technol.* **7** 2101360
- [22] Karimi M B, Mohammadi F and Hooshyari K 2019 Recent approaches to improve nafion performance for fuel cell applications: a review *Int. J. Hydrogen Energy* **44** 28919–38
- [23] Naji L, Chudek J A and Baker R T 2008 Magnetic resonance imaging study of a soft actuator element during operation *Soft Matter* **4** 1879–86
- [24] Rasouli H, Naji L and Hosseini M G 2017 Electrochemical and electromechanical behavior of Nafion-based soft actuators with PPy/CB/MWCNT nanocomposite electrodes *RSC Adv.* **7** 3190–203
- [25] Jung S Y, Ko S Y, Park J O and Park S 2015 Enhanced ionic polymer metal composite actuator with porous nafion membrane using zinc oxide particulate leaching method *Smart Mater. Struct.* **24** 037007
- [26] Yilmaz O C, Sen I, Gurses B O, Ozdemir O, Cetin L, Sarikanat M, Seki Y, Sever K and Altinkaya E 2019 The effect of gold electrode thicknesses on electromechanical performance of nafion-based ionic polymer metal composite actuators *Compos B Eng.* **165** 747–53

- [27] Ru J, Wang Y, Chang L, Chen H and Li D 2016 Preparation and characterization of water-soluble carbon nanotube reinforced Nafion membranes and so-based ionic polymer metal composite actuators *Smart Mater. Struct.* **25** 095006
- [28] Paleo A J, Staiti P, Brigandi A, Ferreira F N, Rocha A M and Lufrano F 2018 Supercapacitors based on AC/MnO₂ deposited onto dip-coated carbon nanofiber cotton fabric electrodes *Energy Storage Mater.* **12** 204–15
- [29] Liu Y, Hu Y, Zhao J, Wu G, Tao X and Chen W 2016 Self-powered piezoionic strain sensor toward the monitoring of human activities *Small* **12** 5074–80
- [30] Xu C et al 2017 Filling the holes in piezopolymers with a solid electrolyte: a new paradigm of poling-free dynamic electrets for energy harvesting *J. Mater. Chem. A Mater.* **5** 189–200
- [31] Cha Y, Abdolhamidi S and Porfiri M 2015 Energy harvesting from underwater vibration of an annular ionic polymer metal composite *Meccanica* **50** 2675–90
- [32] Vinh N D and Kim H M 2017 Ocean-based electricity generating system utilizing the electrochemical conversion of wave energy by ionic polymer-metal composites *Electrochem. Commun.* **75** 64–8
- [33] Zhao Y et al 2018 Improve the performance of mechano-electrical transduction of ionic polymer-metal composites based on ordered nafion nanofibres by electrospinning *Polymers (Basel)* **10** 803
- [34] Krishnamoorthy K, Manoharan S, Mariappan V K, Pazhamalai P and Kim S J 2022 Decoupling mechano- and electrochemical gating: a direct visualization for piezo-ionic propelled proton tunneling in self-charging supercapacitors *J. Mater. Chem. A Mater.* **10** 7818–29
- [35] Liu Y, Hu Y, Zhao J, Wu G, Tao X and Chen W 2016 Self-powered piezoionic strain sensor toward the monitoring of human activities *Small* **12** 5074–80
- [36] Mousavi M S S, Manteghi F and Kolahdouz M 2020 Enhanced actuation application of nafion–ZnO nanoparticles doped sheet as ionic polymer metal composite (IPMC); dopant piezoelectric effect *Bull. Mater. Sci.* **43** 94
- [37] Landi B J, Raffaele R P, Heben M J, Alleman J L, VanDerveer W and Gennett T 2002 Single wall carbon nanotube–nafion composite actuators *Nano Lett.* **2** 1329–32
- [38] Martínez-Huitle C A, Suely Fernandes N, Ferro S, de Battisti A and Quiroz M A 2010 Fabrication and application of Nafion[®]-modified boron-doped diamond electrode as sensor for detecting caffeine *Diam. Relat. Mater.* **19** 1188–93
- [39] Myndrul V, Iatsunskiy I, Babayevska N, Jarek M and Jesionowski T 2022 Effect of electrode modification with chitosan and nafion[®] on the efficiency of real-time enzyme glucose biosensors based on ZnO tetrapods *Materials* **15** 4672
- [40] Lu J, Drzal L T, Worden R M and Lee I 2007 Simple fabrication of a highly sensitive glucose biosensor using enzymes immobilized in exfoliated graphite nanoplatelets nafion membrane *Chem. Mater.* **19** 6240–6
- [41] Olvera D and Monaghan M G 2021 Electroactive material-based biosensors for detection and drug delivery *Adv Drug Deliv Rev* **170** 396–424
- [42] Gibbons E N, Winder C, Barron E, Fernandes D, Krysmann M J, Kelarakis A, Parry A V S and Yeates S G 2019 Layer by layer antimicrobial coatings based on nafion, lysozyme, and chitosan *Nanomaterials* **2019** 9 1563
- [43] Szczęch M, Lopuszyńska N, Tomal W, Jasiński K, Węglarz W P, Warszyński P and Szczepanowicz K 2020 Nafion-based nanocarriers for fluorine magnetic resonance imaging *Langmuir* **36** 9534–9
- [44] Burns W F, Tingey D T, Evans R C and Bates E H 1983 Problems with a Nafion[®] membrane dryer for drying chromatographic samples *J. Chromatogr. A* **269** 1–9
- [45] Chen Y, Zhong Q, Li G, Tian T, Tan J and Pan M 2018 Electrochemical study of temperature and Nafion effects on interface property for oxygen reduction reaction *Ionics (Kiel)* **24** 3905–14
- [46] Ngo T T, Yu T L and Lin H L 2013 Nafion-based membrane electrode assemblies prepared from catalyst inks containing alcohol/water solvent mixtures *J. Power Sources* **238** 1–10
- [47] Pazhamalai P, Krishnamoorthy K, Manoharan S, Mariappan V K and Kim S J 2022 Monolithic integration of MoS₂ quantum sheets on solid electrolyte for self-charging supercapacitor power cell governed by piezo-ionic effect *Sustain. Mater. Technol.* **33** e00459
- [48] Wang A C, Wu C, Pisignano D, Wang Z L and Persano L 2018 Polymer nanogenerators: opportunities and challenges for large-scale applications *J. Appl. Polym. Sci.* **135** 1–17
- [49] Chen A, Zhang C, Zhu G and Wang Z L 2020 Polymer Materials for high-performance triboelectric nanogenerators *Adv. Sci.* **2000186** 1–25
- [50] Gonçalves R, Tozzi K A, Saccardo M C, Zuquello A G and Scuracchio C H 2020 Nafion-based ionomeric polymer/metal composites operating in the air: theoretical and electrochemical analysis *J. Solid State Electrochem.* **24** 1845–56
- [51] Jo C, Pugal D, Oh I K, Kim K J and Asaka K 2013 Recent advances in ionic polymer-metal composite actuators and their modeling and applications *Prog. Polym. Sci.* **38** 1037–66
- [52] Hamid N S A, Kamarudin S K and Karim N A 2021 Potential of Nafion/eggshell composite membrane for application in direct methanol fuel cell *Int. J. Energy Res.* **45** 2245–64
- [53] Sigwadi R, Dhlamini M S, Mokrani T, Nemavhola F, Nonjola P F and Msomi P F 2019 The proton conductivity and mechanical properties of Nafion[®]/ZrP nanocomposite membrane *Heliyon* **5** e02240
- [54] Vchirawongkwin V, Pornpiganon C, Kritayakornupong C, Tongraar A and Rode B M 2012 The stability of bisulfite and sulfonate ions in aqueous solution characterized by hydration structure and dynamics *J. Phys. Chem. B* **116** 11498–507
- [55] Gruger A, Régis A, Schmatko T and Colomban P 2001 Nanostructure of Nafion[®] membranes at different states of hydration: an IR and Raman study *Vib. Spectrosc.* **26** 215–25
- [56] Hsu C-C, Tran T T, van, Kumar S R and Lue S J 2019 Highly permeable transition metal ions through perfluorosulfonate cation-exchange membrane *Polym. Bull.* **76** 6257–74
- [57] Kosseoglou D, Kokkinofa R and Sazou D 2011 FTIR spectroscopic characterization of Nafion[®]-polyaniline composite films employed for the corrosion control of stainless steel *J. Solid State Electrochem.* **15** 2619–31
- [58] Laporta M, Pegoraro M and Zanderighi L 1999 Perfluorosulfonated membrane (Nafion): FT-IR study of the state of water with increasing humidity *Phys. Chem. Chem. Phys.* **1** 4619–28
- [59] Yang R, Qin Y, Li C, Dai L and Wang Z L 2009 Characteristics of output voltage and current of integrated nanogenerators *Appl. Phys. Lett.* **94** 22905
- [60] Cha S N, Seo J S, Kim S M, Kim H J, Park Y J, Kim S W and Kim J M 2010 Sound-driven piezoelectric nanowire-based nanogenerators *Adv. Mater.* **22** 4726–30
- [61] Stassi S, Cauda V, Ottone C, Chiodoni A, Pirri C F and Canavese G 2015 Flexible piezoelectric energy nanogenerator based on ZnO nanotubes hosted in a polycarbonate membrane *Nano Energy* **13** 474–81
- [62] Sultana A, Alam M M, Garain S, Sinha T K, Middya T R and Mandal D 2015 An effective electrical throughput from PANI supplemented zns nanorods and PDMS-based flexible piezoelectric nanogenerator for power up portable electronic devices: an alternative of MWCNT Filler *ACS Appl. Mater. Interfaces* **7** 19091–7

- [63] Xiao T X, Jiang T, Zhu J X, Liang X, Xu L, Shao J J, Zhang C L, Wang J and Wang Z L 2018 Silicone-based triboelectric nanogenerator for water wave energy harvesting *ACS Appl. Mater. Interfaces* **10** 3616–23
- [64] Aminullah K A K, Kasi J K, Uddin M and Bokhari M 2020 Triboelectric nanogenerator as self-powered impact force sensor for falling object *Curr. Appl Phys.* **20** 137–44
- [65] Ding X, Cao H, Zhang X, Li M and Liu Y 2018 Large scale triboelectric nanogenerator and self-powered flexible sensor for human sleep monitoring *Sensors (Switzerland)* **18** 1713
- [66] Kim Y, Wu X and Oh J H 2020 Fabrication of triboelectric nanogenerators based on electrospun polyimide nanofibers membrane *Sci. Rep.* **10** 1–9